JOURNAL OF SOLID STATE CHEMISTRY **101**, 309–321 (1992)

Comparison of the Crystal Structures of γ-Bi_2MoO_6 and Bi_2WO_6

JOHN G. THOMPSON,* SIEGBERT SCHMID, AND RAY L. WITHERS

Research School of Chemistry, Australian National University, G.P.O. Box 4, Canberra, ACT 2601, Australia

A. DAVID RAE

School of Chemistry, University of New South Wales, P.O. Box 1, Kensington, NSW 2033, Australia

AND JOHN D. FITZ GERALD

Research School of Earth Sciences, Australian National University, G.P.O. Box 4, Canberra, ACT 2601, Australia

Received December 26, 1991; accepted May 11, 1992

The crystal structure of γ-Bi_2MoO_6, koechlinite, is compared with the recently re-refined structure of Bi_2WO_6, russellite. Appropriate resetting of the atomic coordinates of γ-Bi_2MoO_6 showed the structures to be isomorphous. Symmetry decomposition of these structures shows the major displacive modes to be virtually identical. The magnitude and/or sign of some of the minor displacive modes, however, are not in agreement. The advantages of X-ray diffraction data over neutron powder data for the refinement of these minor modes are discussed. Transmission electron microscope evidence is presented for the existence of a minority $B1a1$ component coherently intergrown with the majority $P2_1ab$ structure in γ-Bi_2MoO_6, as also observed in Bi_2WO_6. To obtain evidence of the recently reported structural phase transition in Bi_2WO_6 at ~15°C, diffraction patterns and images of this material were recorded at low temperature. The coherent intergrowths were still found to occur at low temperature.

Introduction

The crystal structures of γ-Bi_2MoO_6 (*1–4*), with the mineral name koechlinite, and Bi_2WO_6 (*5*, *6*), with the mineral name russellite, have been previously determined (see Fig. 1). Bi_2WO_6, an $n = 1$ member of the family of Aurivillius phase, $Bi_2O_2 \cdot A_{n-1}B_nO_{3n+1}$, was of interest for its physical property of strong ferroelectricity. γ-Bi_2MoO_6 was also studied because of this property but in addition as a very selective catalyst for alkene oxidation.

In previous crystal structure studies on each of these compounds the only analogy drawn between the two was by Theobald *et al.* (*4*), who recognized the similar unit cell dimensions but who noted that the reported space group, *B2ab* (*6*), was different from all the possible space groups previously con-

* To whom correspondence should be addressed.

0022-4596/92 $5.00

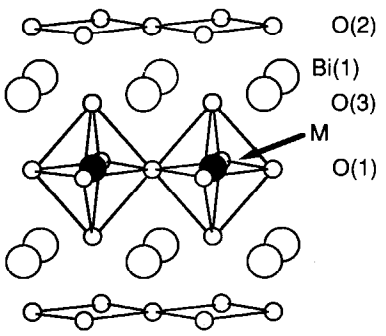

FIG. 1. A perspective drawing, approximately down ⟨110⟩, of the undistorted *Fmmm* parent structure common to Bi_2WO_6 and γ-Bi_2MoO_6. Only atoms between $\frac{1}{4}\mathbf{c}$ and $\frac{3}{4}\mathbf{c}$ are shown. M = Mo, W.

sidered for γ-Bi_2MoO_6. The concurrent, and apparently completely independent, neutron powder diffraction studies of γ-Bi_2MoO_6 by Teller *et al.* (*3*) and Theobald *et al.* (*4*), using time-of-flight and monochromated neutrons, respectively, cleared up the controversy over its space group symmetry. Both arrived at the same result within experimental error, this result giving much more plausible O–O distances than the earlier Van den Elzen and Rieck single-crystal X-ray diffraction study (*1*). Both neutron powder studies determined that the correct space group was $Pca2_1$ as proposed by Van den Elzen and Rieck (*3*), though an unfortunate typographical error in the abstract of the paper by Teller *et al.* (*3*) indicated $Pna2_1$.

The earlier neutron powder diffraction study of Bi_2WO_6 (*6*), as mentioned above, gave the space group for this structure as *B2ab*. However, our recent re-refinement of this structure (*5*) using single-crystal X-ray diffraction data in conjunction with careful transmission electron microscopy (TEM) dark field imaging and electron diffraction studies on the same material determined the space group to be $P2_1ab$ (a nonstandard setting of $Pca2_1$, chosen so as to be consistent with the convention of preserving the **a** axis as the polar axis). Subsequently the authors have realized the analogy between the two structures. This paper attempts to illustrate not only that the structures are in remarkable agreement with each other, at least in terms of the major displacive features, but also that synthetic crystals of γ-Bi_2MoO_6, like Bi_2WO_6, show coherent intergrowths of two distinct modulated variants.

Experimental

Materials

γ-Bi_2MoO_6 was prepared both by solid state reaction of the component oxides and by coprecipitation. In the former synthetic route stoichiometric quantities of Bi_2O_3 (99.999%, Atomergic) and MoO_3 (99.999%, Halewood Chemicals) were thoroughly mechanically mixed under acetone using a mortar and pestle. The specimen was progressively heated in an alumina vessel in air at 550°C for 5 days until XRD showed the existence of a single, well-crystallized orthorhombic phase, pale yellow in color. The final heating regime was 600°C for 1 day followed by 550°C for 3 days. XRD showed no further change with this final heating. The latter synthetic route involved coprecipitation from stoichiometric solutions of $(NH_4)_6Mo_7O_{24} \cdot 4H_2O$ (May & Baker, AR) and $Bi(NO_3)_3 \cdot 5H_2O$ (Ajax, AR), similar to the method described by Matsuura *et al.* (*7*). After initial heating of the precipitate for 1 hr at 290°C and then for 1 hr at 420°C, it was mechanically mixed and then finally heated at 550°C for 22 hr.

In addition to the synthetic specimens, a naturally occurring koechlinite (γ-Bi_2MoO_6) specimen from Horni, Czechoslovakia, was also studied, as previous single-crystal X-ray structure determination (*2*) had been performed on naturally occurring material, in contrast to the more recent neutron powder studies (*3*, *4*) which were performed on synthetic specimens prepared by the coprecipitation method described above. The

TABLE I

REFINED UNIT CELL DIMENSIONS

Compound	a (Å)	b (Å)	c (Å)	V (Å^3)
Bi_2MoO_6, solid state	5.507(2)	5.484(1)	16.214(6)	489.7(2)
Bi_2MoO_6, coprecipitation	5.504(2)	5.485(3)	16.22(1)	489.7(4)
Koechlinite, Horni, Czechoslovakia	5.503(2)[a]	5.503(2)[a]	16.28(2)	493.3(6)
Bi_2WO_6	5.4559(4)	5.4360(4)	16.4298(17)	487.3(1)

[a] Constrained to be equal as no splitting of lines was observed.

Bi_2WO_6 studied by transmission electron microscopy was the same material previously reported by us (*5*).

Characterization

For the synthetic specimens of γ-Bi_2MoO_6 the course of reaction was followed by X-ray powder diffraction (XRD) using a Guinier–Hägg camera with monochromated Cu$K\alpha_1$ radiation. For accurate determination of diffraction lines for the purpose of refining the unit cell dimensions, Si (NBS No. 640) was used as an internal standard. For examination by TEM finely ground specimen was dispersed onto a holey carbon grid. Electron diffraction patterns were recorded using a JEOL 100CX microscope and medium resolution images using a Philips EM430 microscope. The low temperature work was carried out using a Gatan liquid nitrogen cold stage.

Results and Discussion

XRD

The unit cell dimensions of the two synthetic γ-Bi_2MoO_6 specimens and the mineral koechlinite specimen are listed in Table I together with the dimensions of synthetic Bi_2WO_6 (*5*). The XRD lines for the mineral specimen were not sufficiently well resolved to observe the orthorhombic distortion. There is little difference in the unit cell dimensions of the three γ-Bi_2MoO_6 specimens, which, to a first approximation, is indicative of the three specimens being structurally the same. The similarity of the Bi_2WO_6 unit cell dimensions, and in particular the orthorhombic distortion (a/b = 1.004 for both Bi_2MoO_6 and for Bi_2MoO_6), also suggests analogous structure.

TEM

Figure 2 shows selected area electron diffraction patterns (SADP's) of γ-Bi_2MoO_6 down the three major zone axes [010], [100], and [001] as well as down the [2$\bar{1}$0] zone axis. Comparison of these diffraction patterns with those of Bi_2WO_6 in the recent TEM and single-crystal X-ray study by the present authors (*5*) shows them to be analogous in nearly every respect. SADP's of the three γ-Bi_2MoO_6 specimens displayed the same features. It should be noted that γ-Bi_2MoO_6 was significantly more susceptible to electron beam damage than Bi_2WO_6.

As mentioned earlier we have chosen the nonstandard space group $P2_1ab$ in order to comply with the convention used for this family of ferroelectric materials, namely choosing the **a** axis as the polar axis. $Pca2_1$ transforms to $P2_1ab$ by the following permutation of axes: **abc** → **cab** (see Table II). The conditions for $P2_1ab$ are $h0l$: $h = 2n$ and $hk0$: $k = 2n$. As previously discussed for Bi_2WO_6 (*5*) the strongly observed reflections correspond to the underlying $Fmmm$ average structure (see Fig. 1) while the much weaker satellite reflections correspond to $\mathbf{k} = \mathbf{a}^*$, $\mathbf{k} = \mathbf{b}^*$, and $\mathbf{k} = \mathbf{c}^*$ displacive modulations of this underlying, average structure [see Table I of Ref. (*5*)]. Only those displacive modulations compatible with the resultant space group symmetry can have finite amplitude.

The violation of the above extinction conditions for $P2_1ab$ appears to lower the resultant space group symmetry fo $P1a1$. As for Bi_2WO_6, however, the A- and C-centered classes of data ($h + l = 2n + 1$) are streaked

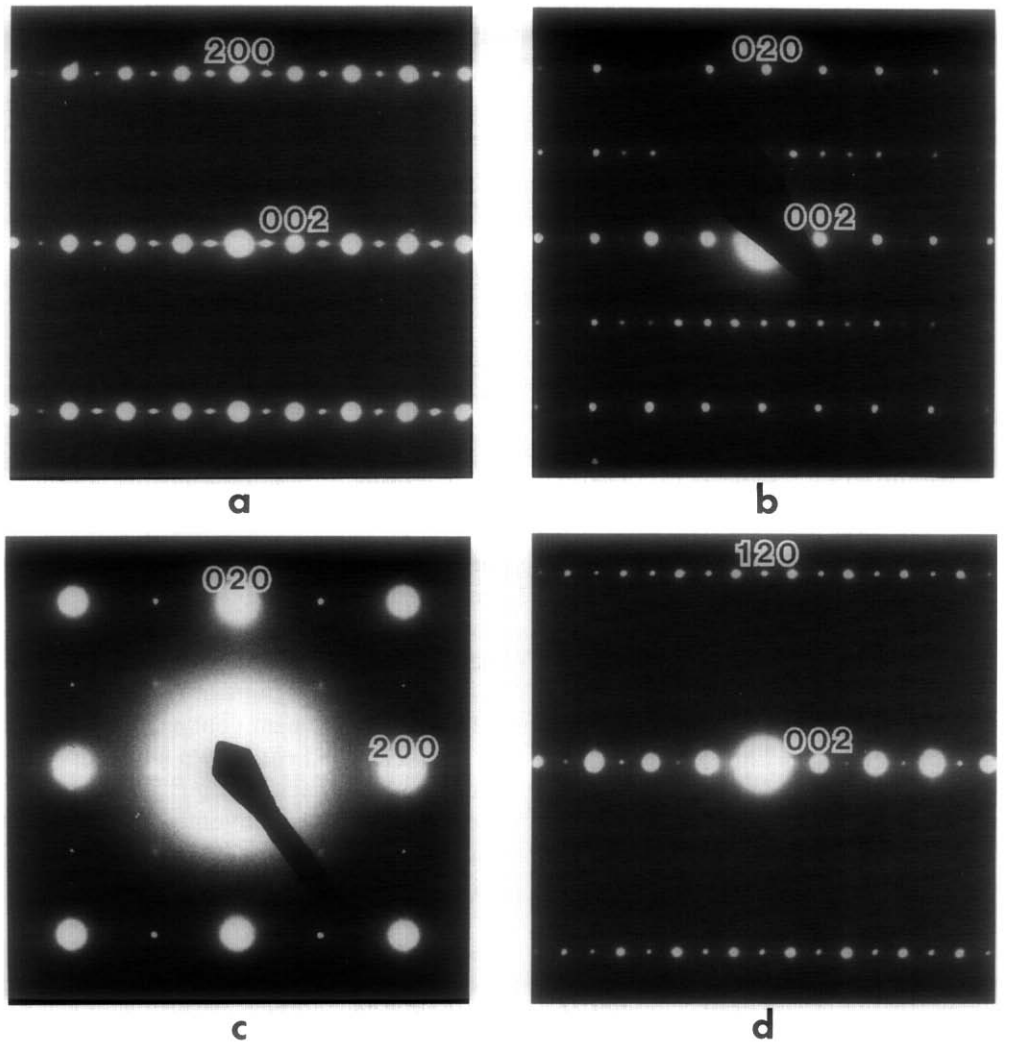

FIG. 2. Typical (a) [010], (b) [100], (c) [001], and (d) [$2\bar{1}0$] zone axis SADP's for γ-Bi_2MoO_6. The streaking of the A- and C-centered classes of data corresponding to the coherent intergrowths, as seen in a, was not always readily visible; see b and d. The $P2_1ab$ forbidden reflections $hk0$: $k = 2n + 1$, however, are clearly visible in c.

along the **c*** direction, consistent with some sort of planar faulting along this direction. Figure 3 shows a bright field image down the [$2\bar{1}0$] zone axis of γ-Bi_2MoO_6 (coprecipitated specimen), there appearing to be a coherent intergrowth of two different structures with **c** axis periodicities of ~16 Å (majority component) and ~8 Å (minority component). The same feature was observed for Bi_2WO_6. These two coherently intergrown structures result from the local coexistence of different displacive modes. The coexistence of these various modes reduces the symmetry of the *Fmmm* parent structure to $P2_1ab$ and $B1a1$ space group symmetries, respectively, with common

TABLE II

RESETTING REPORTED Bi_2MoO_6 STRUCTURES FROM $Pca2_1$ TO $P2_1ab$

$(x\mathbf{a} + y\mathbf{b} + z\mathbf{c})$ (3) $\rightarrow$ $\{(z + 0.0145)\mathbf{a} + x\mathbf{b} - (y + 0.25)\mathbf{c}\}$ (5)
$(x\mathbf{a} + y\mathbf{b} + z\mathbf{c})$ (4) $\rightarrow$ $\{(z + 0.0140)\mathbf{a} + x\mathbf{b} - (y + 0.25)\mathbf{c}\}$ (5)
$(x\mathbf{a} + y\mathbf{b} + z\mathbf{c})$ (1) $\rightarrow$ $\{(z + 0.0238)\mathbf{a} + x\mathbf{b} - (y + 0.25)\mathbf{c}\}$ (5)

Symmetry operations	
Bi_2MoO_6 refinements (1, 2, 4)	Bi_2WO_6 refinement (5)
(i) x, y, z	(i) x, y, z
(ii) $\frac{1}{2} - x, y, \frac{1}{2} + z$	(ii) $\frac{1}{2} + x, -y, \frac{1}{2} - z$
(iii) $\frac{1}{2} + x, -y, z$	(iii) $\frac{1}{2} + x, \frac{1}{2} - y, z$
(iv) $-x, -y, \frac{1}{2} + z$	(iv) $x, \frac{1}{2} + y, \frac{1}{2} - z$

Bi_2MoO_6 label (1, 3, 4)		Bi_2WO_6 label (5)
Bi(1)i	$\rightarrow$	Bi(1')i
Bi(2)i	$\rightarrow$	Bi(1)i
Mo(1)i	$\rightarrow$	W(1)i
O(1)i	$\rightarrow$	O(3)i
O(2)i	$\rightarrow$	O(2')iv
O(3)i	$\rightarrow$	O(2)i
O(4)i	$\rightarrow$	O(1')i
O(5)i	$\rightarrow$	O(1)i
O(6)i	$\rightarrow$	O(3')iii

axial lengths for **a**, **b**, and **c**. The major displacive modes present in these variants are of *F2mm*, *Bmab*, and *Abam* symmetries for a resultant space group symmetry of $P2_1ab$ and of *F2mm*, *Bmab*, and *Bbam* symmetries for a resultant space group symmetry of $B1a1$. In structural terms, the *Abam* and *Bbam* distortion modes both involve rotations of corner-linked planes of MoO_6 octahedra about axes parallel to **c** but differ in the translational arrangement (A or B centering) relating adjacent layers. Figure 4 shows a schematic representation of the atomic displacement patterns involved in these major modes. For a full discussion refer to Rae *et al.* (5).

It should be remembered that the material used in the two neutron powder refinements of the γ-Bi_2MoO_6 structure was prepared by the same coprecipitation method used for the material studied in the present work. Electron diffraction patterns from most crystals showed the same streaked, $P2_1ab$ forbidden reflections to be present. It must, therefore, be concluded that intergrowths of the minority $B1a1$ structure were present in the material used in the two neutron powder refinements. While the presence of small, coherent domains of this second structure would have a greater effect on the observed intensities for neutrons than for X-rays (the displacements are due exclusively to oxygen shifts), the observation of weak, and probably broad, space group forbidden reflections would be difficult in a powder profile unless one was looking for them.

Symmetry Decomposition of Reported Structures of γ-Bi_2MoO_6

As discussed above, there have been two neutron powder studies of the structure and several earlier single-crystal X-ray studies, though we will only discuss the X-ray structure of Van den Elzen and Rieck (1) as it is the only X-ray study that used the correct space group.

For the purpose of comparison with the recent structure refinement of Bi_2WO_6 (5) we have reset the origins and orientations of the reported γ-Bi_2MoO_6 structures and relabeled atoms as detailed in Table II. The origin is chosen so that all symmetry operations are unchanged from those appropriate to the *Fmmm* parent symmetry.

Theobald *et al.* (4) discussed the possible resultant space groups for γ-Bi_2MoO_6 using what was essentially a normal mode analysis. They allowed for three types of distortion away from the high symmetry parent structure. In our setting, their type 1 motion corresponds to rotation of MoO_6 octahedra around **c**, giving rise to either *Abam* or *Bbam* symmetry, dependent upon the centering across the Bi_2O_2 layers (see Fig. 4c). Their type 2 motion corresponds to rotation of MoO_6 octahedra around **a**, leading to either *Bmab* or *Amaa* symmetry, again dependent upon the centering across the Bi_2O_2 layers (see Fig. 4b). Combining type 1 and type 2 motions then led them to four possible centrosymmetric resultant space groups. Destruction of the center of inversion via

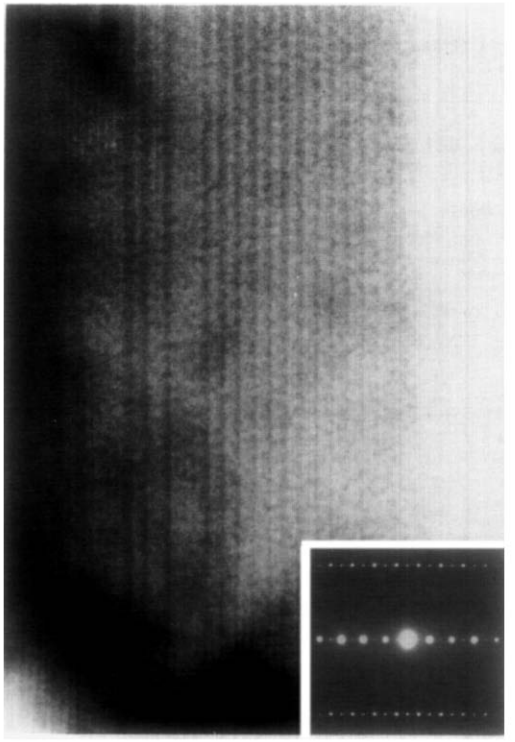

FIG. 3. Bright field image of γ-Bi_2MoO_6 with corresponding selected area electron diffraction pattern (inset) along the [$2\bar{1}0$] zone axis. This image shows coherent intergrowth between two distinct modulated variants, though the 8 Å spacings are not as clearly visible as those in Bi_2WO_6 (*5*), due principally to the difficulty in obtaining suitable images because of very rapid electron beam damage.

the addition of their type 3 motion (of *F*2*mm* symmetry—see Fig. 4a) then gave them possible resultant space groups, one of which corresponds to the correct observed space group.

A decomposition of the reported structures in terms of the various displacive modes of different symmetries is presented in Table III. The displacive modes involving rotation of the MoO_6 octahedra can also be quantified in terms of rotation angle. These angles are listed in Table IV.

There are three features which are evident from examination of the tabulated data.

1. Within the uncertainties for their respective atomic positional parameters, the two independent neutron powder refinements are essentially identical.

2. The earlier X-ray refinement of Van den Elzen and Rieck (*1*) was in general agreement with the later neutron work except for the sign on the x axis shifts of the O(2′) and O(3′) atoms, and this can be unequivocally described as an error. In terms of normal mode analysis the error creates a large *Ccma* displacive component for these atoms while reducing the *F*2*mm* component, (see Table III). The magnitude of the *Ccma* displacive mode is greatly diminished by correcting the sign error. Monitoring the C-centered data (*hkl* eeo and oee, e for even and o for odd) would have highlighted the distinction between the correct and incorrect options. Their refinement used a single isotropic thermal parameter common to all the oxygen atoms and the absence of individual atom anisotropic refinement stabi-

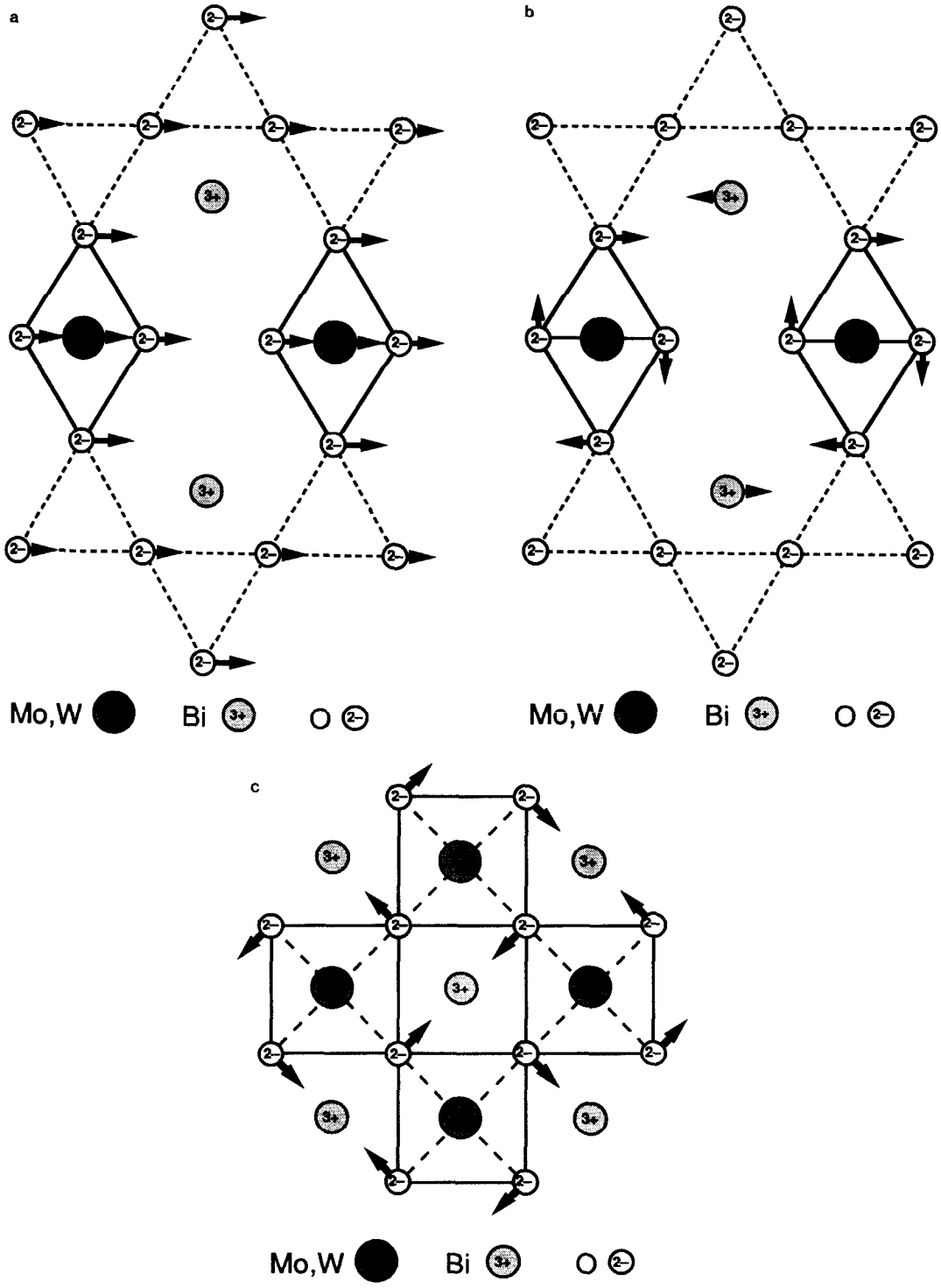

FIG. 4. Schematic representation of the atomic displacement patterns for the major displacive modes having *F*2*mm* (a), *Bmab* (b), and *Abam* (c) symmetry. The *F*2*mm* component corresponds to the spontaneous polarization along **a**. The *Bmab* and *Abam* components involve rotation of the MO_6 (M = Mo, W) octahedra about **a** and **c**, respectively.

TABLE III

DISPLACIVE COMPONENTS FOR THE DISPLACIVE MODES OF Bi_2WO_6 AND γ-Bi_2MoO_6 (FRACTIONAL COORDINATES × 10^4)

Atom label	Ref.	*F2mm*		*Bmab*		*Abam*		*Amam*		*Ccma*	*Bbab*	*Cmma*
		Δx	Δy	Δy	Δz	Δx	Δy	Δy	Δz	Δx	Δy	Δz
Mo(1)	(3)	145						28				12
	(4)	140						10				21
	(1)	238						99				14
W(1)	(5)	209						79				0[a]
Bi(1)	(3)	0[a]		−179				1		42		−8
	(4)	0[a]		−180				10		30		−9
	(1)	0[a]		−205				17		32		0
	(5)	0[a]		−200				9		40		0[a]
Bi(1′)	(3)	0[a]		179				1		−42		−8
	(4)	0[a]		180				10		−30		−9
	(1)	0[a]		205				17		−32		0
	(5)	0[a]		200				9		−40		0[a]
O(1)	(3)	682	102		−156	513	−481					22
	(4)	695	45		−164	545	−475					39
	(1)	763	105		−145	475	−465					−5
	(5)	635	87		−152	406	−388					0[a]
O(1′)	(3)	682	−102		156	−513	−481					22
	(4)	695	−45		164	−545	−475					39
	(1)	763	−105		145	−475	−465					−5
	(5)	635	−87		152	−406	−388					0[a]
O(2)	(3)	365			6		−23		−12	−56	−117	
	(4)	355			−2		5		−46	5	−85	
	(1)	18[b]			5		−50		−5	320[b]	50	
	(5)	333			4		0		−2	−44	−114	
O(2′)	(3)	365			−6		−23		−12	56	117	
	(4)	355			2		5		−46	−5	85	
	(1)	18[b]			−5		−50		−5	−320[b]	−50	
	(5)	333			−4		0		−2	44	114	
O(3)	(3)	974		605				−49		130		2
	(4)	970		605				−115		80		−15
	(1)	283[b]		680				−290		945[b]		10
	(5)	933		586				82		44		0[a]
O(3′)	(3)	974		−605				−49		−130		2
	(4)	970		−605				−115		−80		−15
	(1)	283[b]		−680				−290		−945[b]		10
	(5)	933		−586				82		−44		0[a]

[a] Constrained to be zero.

[b] Changing the sign of the overall x displacement for O(2′) and O(3′) exchanges the magnitudes of the *F2mm* and *Ccma* components: for O(2) 18 → 320, 320 → 18; for O(2′) 18 → 320, −320 → −18; for O(3) 283 → 945, 945 → 283; and for O(3′) 283 → 945, −945 → −283.

lized the refinement error by assisting the *Fmmm* component to dominate the *F2mm* component by removing degrees of freedom from the refinement pathway. Poorly behaved anisotropic thermal parameters are an essential feature of the refinement of incorrectly phased atom displacements. This behavior has been discussed elsewhere (*8*).

TABLE IV

ROTATION ANGLES OF MoO_6 OCTAHEDRA ABOUT THE **a** AND **c** AXES

Compound	*Bmab* mode (**a** axis)	*Abam* mode (**c** axis)	Ref.
γ-Bi_2MoO_6	10.5°	11.2°	(3)
γ-Bi_2MoO_6	10.8°	11.5°	(4)
Bi_2WO_6	10.3°	9.1°	(5)

3. The recent single-crystal X-ray refinement of Bi_2WO_6 (5) gives a strikingly similar result to those of γ-Bi_2MoO_6 determined by neutron powder diffraction. Not surprisingly, there are some small differences in the magnitudes of the displacive modes, but the signs of displacments on all the atoms for all the major modes (i.e., *F*2*mm*, *Bmab*, and *Abam*) are in agreement. However, the *y* displacements on the O(3) and O(3′) atoms have an opposite sign to those observed in Bi_2WO_6 for the relatively minor (i.e., induced) *Amam* mode and it is obviously necessary to evaluate the reliability of the minor modes and to compare the merits of single-crystal X-ray data and powder diffraction neutron data.

The absence of anomalous dispersion in neutron diffraction data is a very definite handicap for determining the overall phase and finer details of the minor displacement modes. There are two possibilities, either (a) errors in the phases of displacement parameters for the minor modes are self-correcting or (b) comparative refinement is required. Experimentation is the only way of ascertaining refinement behavior and the existence of false minima. Self-correction is unlikely. In the X-ray refinement of Bi_2WO_6 (5) only the *Bbab* mode was self-correcting, and comparative refinement had to be used to ascertain the optimum least-squares refinement.

In neutron refinement the similarity of scattering lengths implies the average contribution of displacive motions to intensity is roughly proportional to the square of the displacive amplitudes. Consequently the minor modes contribute very little to the overall intensity (1 to 2% say) and the lack of anomalous dispersion means correlation between modes is minimized. While the large displacments are well determined, it is hard to go past the conclusion that the contribution of the minor modes contains a large noise component and comparative refinement would be very difficult. Analysis of apparent valences (see below) calculated for the various models confirms that careful X-ray refinement gives a more reliable estimate of the displacement of anomalously scattering atoms away from positions of high symmetry. In the present structures the origin was determined by the overall phase of the *Bmab* and *Abam* modes. For neutron diffraction the polarity direction chosen correlates with the *Bmab* and *Abam* modes to create an initial phase estimate for the *Amam* and *Bbab* modes. This is not an oversubstantial contribution and accounts for the lack of definition in these modes as judged by apparent valence calculations of the refined neutron diffraction structures of γ-Bi_2MoO_6.

Phase Transition near Room Temperature in Bi_2WO_6

Very recently Hirose and colleagues (*9–11*) have reported the existence of anomalous behavior in Bi_2WO_6 at about 15°C in the temperature dependence of various physical properties measured along the **c** axis, such as the dielectric constant and the electric conductivity, as well as in the temperature-dependent behavior of certain diffraction peaks. Such anomalous behavior was found only when measurements were taken along the **c**-axis direction and was interpreted in terms of a first-order displacive structural phase transition although one in which the space group (*Aba*2 in their setting which is equivalent to *B*2*ab* in our setting) does not alter.

In light of these reports of a structural phase transition at ~15°C, a low temperature TEM study was made of Bi_2WO_6 to see whether the previously reported room temperature observation of coherent intergrowths of $P2_1ab$ and $B1a1$ displacively modulated variants (*5*) still held at low temperature. Given that this observation was made at room temperature it was possible that the two modulated variants observed may have represented the high (>15°C) and low temperatures (<15°C) forms of Bi_2WO_6 implied by the electrical anomalies observed by Hirose *et al.* (*9*).

Figure 5a shows a typical satellite dark field image of Bi_2WO_6 taken near the $[2\bar{1}0]$ zone axis at liquid nitrogen temperature—the corresponding $[2\bar{1}0]$ zone axis SADP is shown in Fig. 5b. Clearly the two distinct modulated variants are still present at liquid nitrogen temperatures and cannot be associated with any anomalous behavior of physical properties in the vicinity of 15°C. This is confirmed by the characteristic streaking of the A- and C-centered classes of data visible in the $[2\bar{1}0]$ and [100] zone axis SADP's (obtained at liquid nitrogen temperature) shown in Figs. 5b and 5c.

Bond Valence Considerations

In our recent re-refinements of several Aurivillius phases, $Bi_4Ti_3O_{12}$ (*8*), Bi_3TiNbO_9 (*12*), $Bi_2SrTa_2O_9$ (*13*), and Bi_2WO_6 (*5*), we have used the calculation of bond valences (*14*, *15*) or apparent valences (AVs) (*16*) to discriminate between false and true refinement minima. These calculations were not used as part of the refinement. Rather they were used to justify conclusions reached solely from the quality of X-ray data refinement considerations. In conjunction with a modulated structure approach, we have also used AVs to help explain the driving force for the symmetry-lowering structural distortions observed in these compounds. We shall now use AV calculations to compare X-ray and neutron diffraction refinements and to suggest a simple modification to the Bi_2WO_6 structure that includes a component of the hitherto excluded *Cmma* mode and improves the AV description.

AVs are presented for the three γ-Bi_2MoO_6 structure refinements together with those for Bi_2WO_6 in Table V. As for Bi_2WO_6 (*5*) a noticeable feature is that the AVs for the oxygen atoms on either side of the Bi atom layer, i.e., O(2), O(2′) and O(3), O(3′), appear to be overbonded and underbonded, respectively, while the Bi atom is satisfactorily bonded. This feature is common to all the Aurivillius phases (17) and is believed to be due to the inability of the AV method to deal with lone pairs of electrons in anisotropic structural environments. The remaining AVs all appear to be reasonable, especially when they are averaged between atoms that would be equivalent for the *Fmmm* parent symmetry, e.g., O(1) and O(1′).

The Teller *et al.* refinement (*3*) displays the greatest similarity to Bi_2WO_6 in terms of AVs. The other two refinements differ from these two principally in the AVs for O(3) and O(3′). The incorrect sign on O(2′) and O(3′) in the Van den Elzen and Rieck refinement (*1*) does not have a great effect on the AVs for these two atoms, even though the nonbonding O(1′)–O(3′) interaction (d_{O-O} = 2.2 Å) is implausible as reported by both Theobald *et al.* (*4*) and Teller *et al.* (*3*). AVs are affected only by bonding interactions, and since the O(2′) and O(3′) corrections of 0.2 and 0.4 Å, respectively, are mainly tangential to the bond, the AVs are not greatly affected.

Quality of refinement can be assessed by observing the differences in AVs between atoms that would be equivalent under the parent symmetry. Here it is seen that the Bi_2WO_6 structure determined by X-ray diffraction using a modulated structure approach appears more plausible. This is asso-

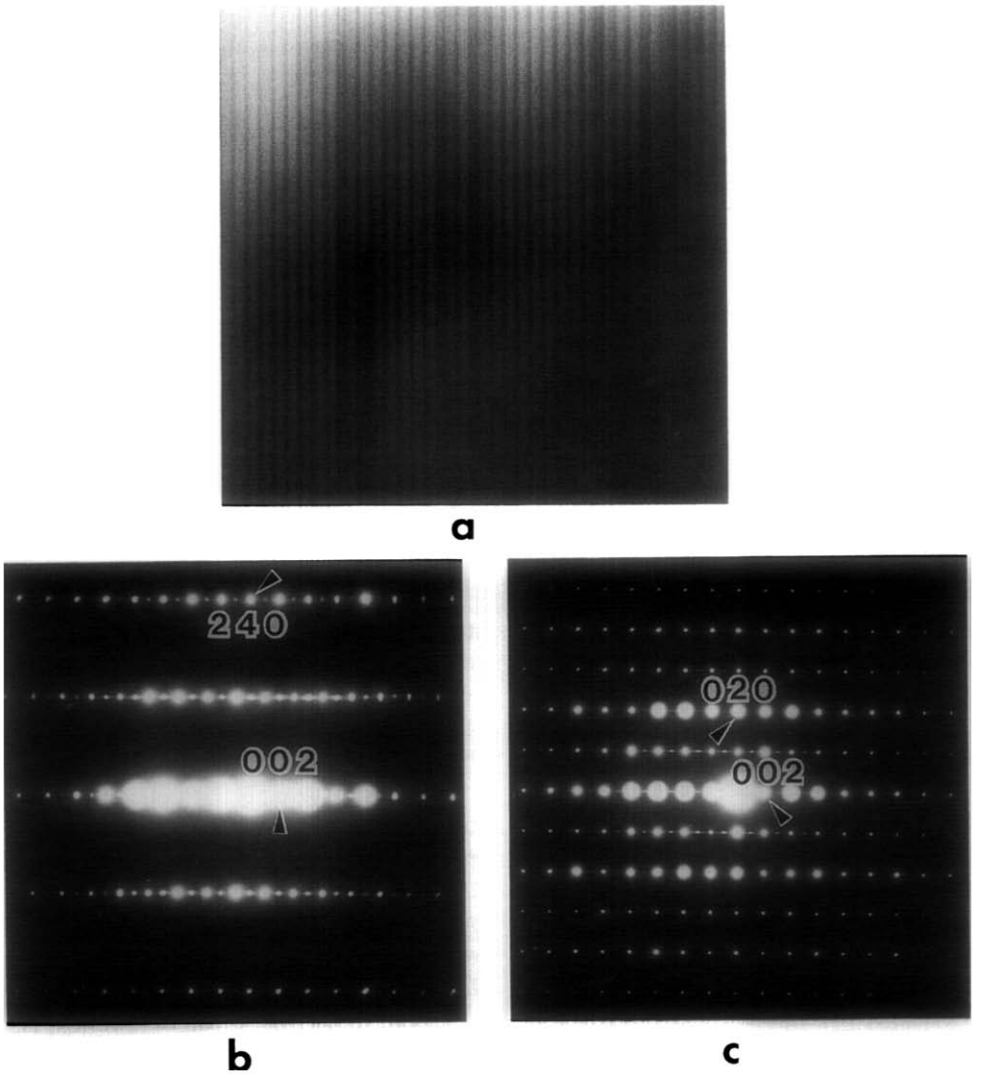

FIG. 5. Typical satellite dark field image (a) of Bi_2WO_6 taken near the [2$\bar{1}$0] zone axis at liquid nitrogen temperature—the corresponding [2$\bar{1}$0] zone axis SADP is shown in (b). The characteristic streaking of the A- and C-centered classes of data is visible in both the [2$\bar{1}$0] (b) and the [100] (c) zone axis SADP's.

ciated with the reliability of the minor modes as the major modes are in essential agreement. Indeed, the only large discrepancy for Bi_2WO_6 is between the value of 2.11 for O(1) and that of 1.95 for O(1′). Incorporation of a 0.005 fractional coordinate correction (0.08 Å) for the O(1) and O(1′) atoms to change the z coordinates to 0.4798 and 0.5102, respectively, produces the AVs listed as "(5)(mod)" in Table V. The values for O(1) and O(1)′ become 2.06 and 1.99 while the difference between the values for Bi(1) and Bi(1′) changes sign but not magnitude.

TABLE V

APPARENT VALENCES[a] FOR ATOMS IN Bi_2WO_6 AND Bi_2MoO_6

Bi_2WO_6 label (5)	γ-Bi_2MoO_6 label (1, 3, 4)	Bi_2WO_6 (5)	Bi_2WO_6 (5)(mod)	γ-Bi_2MoO_6 (3)	γ-Bi_2MoO_6 (4)	γ-Bi_2MoO_6 (1)
Bi(1)	Bi(2)	3.18	3.16	3.11	2.99	3.16
Bi(1')	Bi(1)	3.16	3.18	3.06	3.15	3.13
W(1)	Mo(1)	6.06	6.04	6.05	5.93	5.93
O(1)	O(5)	2.11	2.06	1.95	1.84	2.09
O(1')	O(4)	1.95	1.99	2.05	2.00	1.97
O(2)	O(3)	2.31	2.31	2.35	2.39	2.27
O(2')	O(2)	2.31	2.31	2.26	2.19	2.24
O(3)	O(1)	1.86	1.86	1.87	2.00	1.97
O(3')	O(6)	1.85	1.85	1.74	1.65	1.68

[a] $R_{0(Bi-O)} = 2.094$; $R_{0(W-O)} = 1.900$; $R_{0(Mo-O)} = 1.907$.

One is led to surmise that the apparent discrepancies between parent symmetry-related atoms, evident in their AVs, result from the large uncertainties associated with the experimental determination of the minor displacive modes (discussed above). The same applies to the discrepancies in AVs associated with the differences in the minor displacive modes between the otherwise isomorphous structures compared in this present study (see Table V).

Conclusions

The resetting and the subsequent symmetry decomposition of the reported crystal structure of γ-Bi_2MoO_6 enabled us to readily compare it with the recently re-refined structure of Bi_2WO_6. These chemically closely related materials are structurally analogous, in terms of both crystal structure and structural disorder. It is most likely that the apparent differences between the neutron diffraction structures of γ-Bi_2MoO_6 and the X-ray diffraction structure of Bi_2WO_6 are greater than the real differences and that the γ-Bi_2MoO_6 structure should be modified to more resemble the structure of Bi_2WO_6.

As γ-Bi_2MoO_6 and Bi_2WO_6 are isostructural it follows that those physical properties of these two materials which are crystal structure dependent will also be the same or, at least, very similar. Both materials have been independently investigated for their property of ferroelectricity but it has not been recognized that their spontaneous polarizations (P_s) must be very similar. This follows from the similarity in atom displacements for the ferroelectric $F2mm$ displacive mode in each (see Table III). γ-Bi_2MoO_6 has also been studied for its selectivity as a catalyst for the oxidation of alkenes. As Mo and W are chemically very similar, particularly with regard to their redox chemistry, we would expect that Bi_2WO_6 might show similar catalytic behavior.

Finally, it should be noted that, of all the Aurivillius phases that the authors have studied by TEM, only γ-Bi_2MoO_6 and Bi_2WO_6 displayed the coherent intergrowth of the two closely related structures with different ($P2_1ab$ and $B1a1$) space group symmetries. While the property of ferroelectricity will not be affected by the intergrowth of these two structures, having the ferroelectric distortion, i.e., the $F2mm$ displacive mode, in common, one might expect

optical and other electrical properties such as those reported by Hirose *et al.* (*9*) to be affected by these very fine scale intergrowths.

References

1. A. F. van den Elzen and G. D. Rieck, *Acta Crystallogr. Sect. B* **29,** 2436 (1973).
2. F. Pertlik and J. Zemann, *Fortschr. Mineral. Beihefte* **60,** 162 (1982).
3. R. G. Teller, J. F. Brazdil, R. K. Grasselli, and J. D. Jorgensen, *Acta Crystallogr. Sect. C* **40,** 2001 (1984).
4. F. Theobald, A. Laarif, and A. W. Hewat, *Ferroelectrics* **56,** 219 (1984).
5. A. D. Rae, J. G. Thompson, and R. L. Withers, *Acta Crystallogr. Sect. B* **47,** 870 (1991).
6. R. W. Wolfe, R. E. Newnham, and M. I. Kay, *Solid State Commun.* **7,** 1797 (1969).
7. I. Matsuura, R. Schuit, and K. Hirakawa, *J. Catal.* **63,** 152 (1980).
8. A. D. Rae, J. G. Thompson, R. L. Withers, and A. C. Willis, *Acta Crystallogr. Sect. B* **46,** 474 (1990).
9. T. Hirose, M. Kawaminami, and K. Obara, *Phys. Status Solidi A* **124,** 137 (1991).
10. T. Hirose, M. Kawaminami, and K. Obara, *Phys. Status Solidi A* **127,** 541 (1991).
11. M. Arakawa, T. Hirose, and H. Takeuchi, *J. Phys. Soc. Jpn.* **60,** 4319 (1991).
12. J. G. Thompson, A. D. Rae, R. L. Withers, and D. C. Craig, *Acta Crystallogr. Sect. B* **47,** 174 (1991).
13. A. D. Rae, J. G. Thompson, and R. L. Withers, *Acta Crystallogr. Sect. B* **48,** in press.
14. I. D. Brown, *Chem. Soc. Rev.* **7,** 359 (1978).
15. I. D. Brown and D. Altermatt, *Acta Crystallogr. Sect. B* **41,** 244 (1985).
16. M. O'Keeffe, *Struct. Bonding* **71,** 161 (1989).
17. R. L. Withers, J. G. Thompson, and A. D. Rae, *J. Solid State Chem.* **94,** 404 (1991).